

Surface Plasmon Engineering in Graphene Functionalized with Organic Molecules: A Multiscale Theoretical Investigation

Jierong Cheng,^{*,†} Wei Li Wang,[‡] Hossein Mosallaei,[†] and Efthimios Kaxiras[‡]

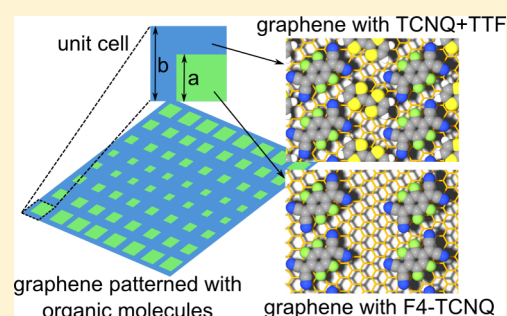
[†]Department of Electrical and Computer Engineering, Northeastern University, Boston, Massachusetts 02115, United States

[‡]Department of Physics and School of Engineering and Applied Sciences, Harvard University, Cambridge, Massachusetts 02138, United States

S Supporting Information

ABSTRACT: Graphene was recently shown to support deep subwavelength surface plasmons at terahertz frequencies characterized by low energy loss and strong field localization, both highly desirable. The properties of graphene can be locally tuned by applying an external gate voltage or by the adsorption of organic molecules that lead to doping through charge transfer. Local tuning of the electronic features of graphene opens the possibility to realize any desired gradient index profile and thus brings large flexibility to control and manipulate the propagation of surface plasmons. Here, we explore this possibility created by functionalizing graphene with organic molecules. We employ a multiscale theoretical approach that combines first-principles electronic structure calculations and finite-difference time-domain simulations coupled by surface conductivity. We show that by patterning two types of organic molecules on graphene, a plasmonic metasurface can be realized with any gradient effective refractive index profile to manipulate surface plasmon beams as desired. The special properties of such devices based on functionalized graphene are compared to the similar metamaterials based on metallic films on top of a gradient index dielectric substrate. Using this idea, we design and analyze an ultrathin broadband THz plasmonic lens as proof-of-concept, while more sophisticated index profiles can also be realized and various plasmonic applications are readily accessible.

KEYWORDS: Surface plasmon, metamaterials, graphene, functionalization, DFT, FDTD



Tailoring electromagnetic response at the micro and nano scales has been a long sought goal that could be reached by artificially structured materials known as metamaterials. Recent advances in metamaterials have enabled a wide range of applications including high-gain nanoantennas,¹ invisibility cloaking,^{2,3} light focusing and collimating,⁴ and beam steering.⁵ These functions can be realized by manipulation of the electromagnetic field through gradient refractive index (GRIN) in space.⁶ To reduce the size and improve the performance of optoelectronic devices, surface plasmons (SP) at the interface of a metal and a dielectric are typically used to manipulate light at the subwavelength scale through collective electron oscillations. The GRIN has been recently extended to manipulate SPs. Because the SP field penetrates into both the metal and the dielectric on either side of the interface, the indices of both materials affect the SP properties. The index of the dielectric can be changed by mixing two materials together with different weights or by drilling air holes of different sizes. By tuning the dielectric part alone, metamaterials for plasmonic applications such as cloaking, concentrators, and beam shifters have been produced.^{7–9} Spatial tuning of the metallic side properties has proven more difficult. Here, we explore a new class of ultrathin plasmonic metasurfaces with any designed GRIN profile based on patterned graphene with organic molecules.

Graphene, a two-dimensional sheet of carbon atoms arranged in a honeycomb lattice, has been observed to support deep subwavelength SPs^{10–13} with highly desirable properties of low energy loss and strong field localization.^{14–16} Tunability is one of the most desirable properties for graphene-based applications. Gate bias provides temporal tunability^{17–20} while patterning molecules enables spatial tunability. Several applications employing gate bias considered so far include modulators,¹⁹ switches,²⁰ and reconfigurable terahertz antennas,¹⁷ but this approach is severely limited when accurate and complex spatial tunability is required. Specifically, if we assume that each discrete element needs to be controlled on the two-dimensional (2D) surface, the path of the gate bias would become complicated, and the field propagation may be affected by the spatially distributed gates. For these reasons, row-by-row control is typically adopted¹⁷ in the local gate bias, and point-by-point control is avoided. In a recent report,¹⁸ however, a design with connected elements is introduced, in which dc bias at one place is used to control all of the elements.

Alternatively, the optical properties of graphene can be tuned through interactions with organic molecules.^{21–24} A variety of

Received: August 10, 2013

Revised: October 29, 2013

Published: November 27, 2013

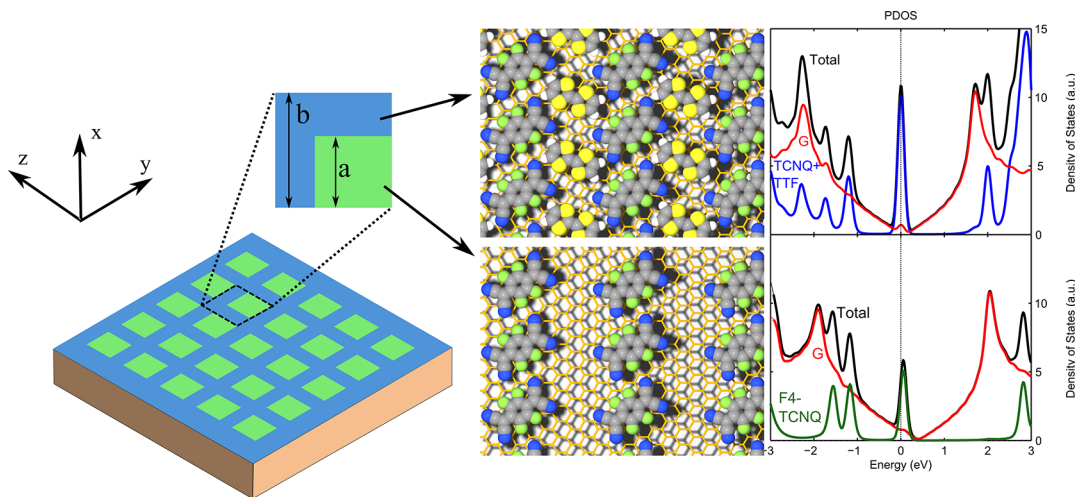


Figure 1. Schematic representation of the graphene structure patterned by organic molecules. The two types of organic molecules used here are TCNQ+TTF (blue area) and F4-TCNQ (green area). The corresponding projected density of states (PDOS) of functionalized graphene areas are plotted with the Fermi level indicated by the dashed vertical line at the zero of the energy scale. The PDOS shows both the effects of doping and the added molecular DOS signature to the total DOS due to the molecule-graphene interactions.

molecules have been shown experimentally to produce n-type or p-type doping in graphene by charge transfer. Using standard patterning processes such as e-beam and dip-pen lithography, it is possible to adsorb molecules on graphene in desired patterns to produce point-by-point spatially tailored features. Figure 1 shows a schematic configuration of the proposed patterned graphene, using two types of molecules, that makes it possible to achieve any desired gradient index profile for the manipulation of SP beams like collimation, bending, focusing and so on. In this work, we investigate the possibility of creating such functionalized graphene metasurfaces using multiscale simulations. We first calculate the optical properties of the graphene–organic molecule complex from first-principles electronic structure methods based on density functional theory (DFT). The calculated surface conductivity is used as input to finite-difference time-domain (FDTD) simulations at the continuum mesoscopic scale to study the SP performance of functionalized graphene. We show that by locally tuning the graphene property point-by-point through molecular patterning, any GRIN profile can be easily achieved. The corresponding SP waves supported by this structure have dispersion properties that are different from traditional metamaterials based on metallic films. We then use the effective medium theory (EMT) approach to construct a proof-of-concept model of patterned-graphene structure as a plasmonic Selfoc lens, and FDTD simulation result confirms its capability of engineering SP propagation.

Our first-principles calculations are carried out using the SIESTA code^{25,26} with the LDA exchange-correlation functional. We use a local-basis set of double- ζ polarized atomic orbitals with an energy cutoff of 70 Ry. The structural relaxations are considered converged when the magnitude of the force on each atom was smaller than 0.01 eV/Å.

All of graphene's atoms are on the same plane that also constitutes its surface. This makes it very susceptible to environment changes such as adsorption of organic molecules.^{21–24} Organic molecules can induce doping in graphene through charge transfer, which shifts the Fermi level and modifies the joint density of states (JDOS) of the system. As shown in Figure 1, two types of organic molecules, TCNQ+TTF and F4-TCNQ, shift the Fermi level of graphene to 0.16

and 0.4 eV respectively with modified PDOS. These changes also affect optical properties by introducing new optical transitions that depend on the coupling strength, directionality and polarization.

Optical transitions in graphene–organic molecule complex are usually characterized by surface conductivity including both interband and intraband contributions. The contribution of interband transitions is computed directly from the electronic structure of the graphene–organic molecule complex with the coupling and occupation of each pair of states involved in a direct transition calculated and summed over all frequencies.²⁷ The intraband contribution to the surface conductivity is accounted for with the Drude model

$$\sigma_{\text{intra}}(\omega) = \frac{i\omega_p^2}{(\omega + i\tau^{-1})} \quad (1)$$

where the relaxation time τ is estimated to be 1 ps based on the experimental data,²⁸ and the plasma frequency ω_p is computed within DFT using²⁹

$$\omega_p^2 = \frac{8\pi e^2}{3\Omega} \sum_{\vec{k}, n} \left| \frac{1}{\hbar} \frac{\partial E_{\vec{k}, n}}{\partial \vec{k}} \right|^2 \delta(E_{\vec{k}, n} - E_F) \quad (2)$$

where \vec{k} is the wave vector, e is the charge of an electron, and Ω is the system volume. E_F and $E_{\vec{k}, n}$ are the Fermi energy and the energy of a state with the summation running over all values of \vec{k} and the band index n . Our calculations show that the additional organic molecule states are mostly nondispersive because of the relatively weak interactions with graphene and with each other. Accordingly, the linear dispersion of the graphene Dirac cone is retained but there is local hybridization of the graphene states and the organic molecule states (see Figure S3 in Supporting Information). Equation 2 shows that the plasma frequency is affected by the dispersion close to the Fermi level, which in turn could be sensitive to the graphene–organic molecule interactions.

Before obtaining the conductivity of molecular doped graphene, the conductivity of purely doped graphene with the ideal band structure is developed to test the technical accuracy of the first-principles DFT calculation. The conductivity is

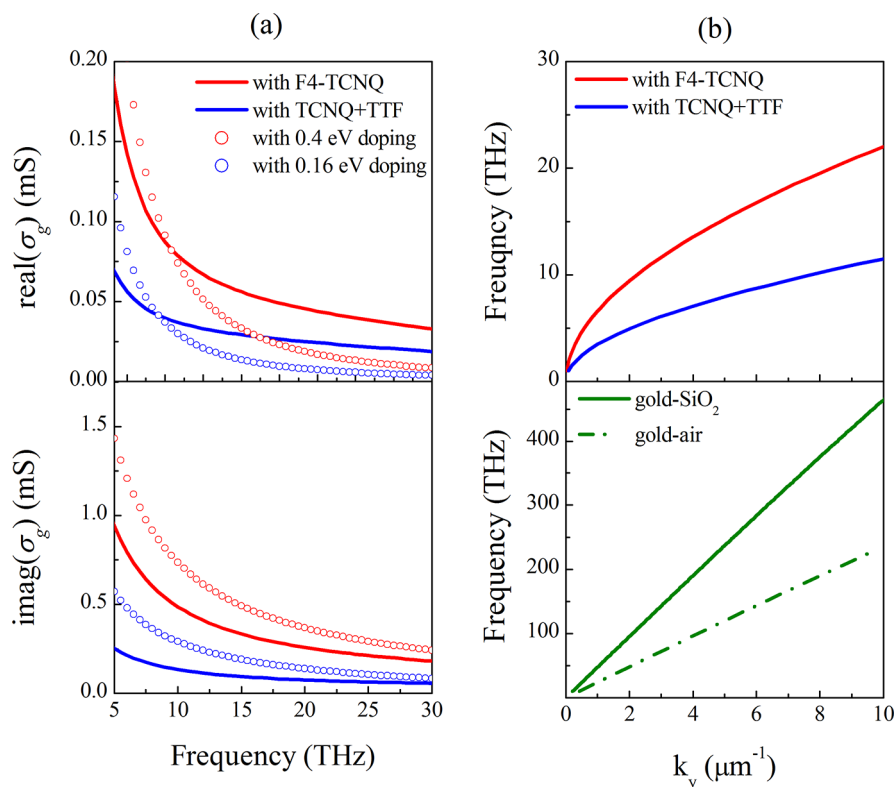


Figure 2. Calculated surface conductivity of functionalized graphene in the terahertz range. (a) The real [$\text{real}(\sigma_g)$] and imaginary [$\text{imag}(\sigma_g)$] parts of the conductivity of graphene doped by F4-TCNQ (red solid lines) and TCNQ+TTF (blue solid lines), calculated from DFT model. The conductivity of pure graphene doped to the same level of 0.4 and 0.16 eV are shown as red and blue circles based on Kubo formula. (b) Dispersion of SPs in functionalized graphene calculated theoretically based on the DFT results (upper panel), the gold–SiO₂ interface and the gold–air interface (lower panel) for comparison.

compared to the analytical Kubo formula,^{30,31} and good agreement can be seen in Figure S1 of Supporting Information. Next, the conductivities of graphene doped by F4-TCNQ and TCNQ+TTF are calculated in Figure 2a. In order to show the effect of molecule–graphene interaction, the conductivities of purely doped graphene with the same Fermi levels (0.4 and 0.16 eV) and relaxation time of 1 ps are shown as a comparison.

As mentioned previously, organic molecules do not only induce charge transfer to shift the Fermi level, but also introduce new optical transitions to modify the transport properties. Thus the conductivity differs from that of the pure graphene doped to the same Fermi level and with the same relaxation time. Specifically, the plasma frequency is modified (reduced in this case) because the interaction of molecules with graphene modifies the band shape at the Fermi level. The reduced plasma frequency leads to smaller conductivity for both real and imaginary parts at the low frequency range (around below 10 THz). At higher frequencies, the real part of σ_g goes above the value for the purely doped case, indicating higher loss for wave propagation. It could be explained by the additional molecular DOS close to the Fermi level in Figure 1. For purely doped graphene, interband transitions impact the optical response only when the frequency satisfies $\hbar\omega > 2\mu_c$.¹⁶ For molecular-doped graphene, however, the interband contribution cannot be neglected even at very low frequencies due to the additional transitions involving the molecular states. The ratio between the real part and imaginary part of σ_g shows that the loss for molecular doped graphene is comparable to that for purely doped graphene at low frequency range, and it increases slightly at higher frequencies due to the interaction between

graphene and molecules. To avoid high loss, we confine the analysis of SP properties to 5–10 THz. (See Figure S5 of Supporting Information for the loss analysis.)

We next study the SP properties in functionalized graphene and how they may be manipulated. We consider a layer of uniformly doped graphene by one type of molecules inserted into the dielectric–dielectric interface. The dispersion relation of SPs at the interface can be calculated from¹⁴

$$-\frac{i\sigma_g}{\omega\epsilon_0} = \frac{\epsilon_{1r}}{\sqrt{k_y^2 - \omega^2\mu_0\epsilon_{1r}\epsilon_0}} + \frac{\epsilon_{2r}}{\sqrt{k_y^2 - \omega^2\mu_0\epsilon_{2r}\epsilon_0}} \quad (3)$$

This expression is derived from Maxwell's equations and proper boundary conditions where the conductivity of graphene σ_g is obtained from DFT calculations in Figure 2a. ϵ_{1r} and ϵ_{2r} are the dielectric constants of the materials above and under the graphene layer, and the free-standing case is considered here for simplicity. k_y is the surface wave vector, and the propagation direction is taken along y with the graphene layer in y – z plane throughout this paper. In the nonretarded region ($k_y \gg \omega(\mu_0\epsilon_0)^{1/2}$), the dispersion relation can be simplified as

$$k_y = \frac{i\omega\epsilon_0(\epsilon_{1r} + \epsilon_{2r})}{\sigma_g} \quad (4)$$

The dispersion relations of SPs are shown in Figure 2b for an infinite graphene sheet with uniform adsorption of F4-TCNQ and TCNQ+TTF molecules, respectively. Clearly, the plasmonic properties in graphene could be changed significantly depending on the species of adsorbed organic molecules.

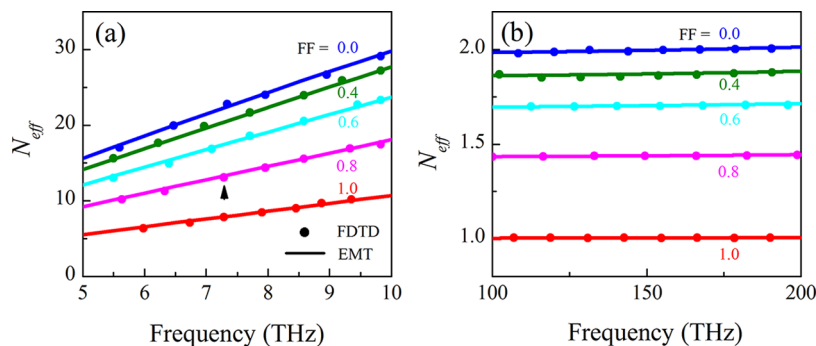


Figure 3. Comparison of calculated effective refractive indices (real part) of metamaterials made of (a) patterned graphene by molecules, and (b) a gold film on top of GRIN dielectric substrate. FF in (b) refers to the relative size of air holes in SiO₂ substrate. For both (a,b), the dots are results from full-wave FDTD simulation and the lines are calculated from EMT with FF ranging from 0.0 to 1.0. The arrow in (a) shows the case studied in the Figure S4 of Supporting Information to explain how it is obtained in FDTD.

The dispersion curves for traditional SPs supported on gold–dielectric interface with the same wave vectors are also shown in Figure 2b as a comparison and will be analyzed in detail later.

The effective refractive index for the SPs can be extracted from the dispersion relation as $n_{\text{eff}} = ck_y/\omega$, which indicates the relative scale of the plasmonic wavelength and the free space wavelength. It is of desire to design a metamaterial with gradually changed effective refractive index profile. However, it is unlikely that molecules with different properties can be used to produce a doping profile in graphene with smooth gradient. It is also not practical from the fabrication point of view to mix various molecules with gradient concentrations. Alternatively, we can implement plasmonic GRIN materials using patterned unit cells made of two different types of organic molecules, yielding an effectively smooth GRIN.³²

The unit cell of graphene metamaterial, as shown in Figure 1, consists of two patches, one with lower Fermi energy in which TCNQ+TTF molecules are adsorbed (blue region), and one with higher Fermi energy in which F4-TCNQ molecules are adsorbed (green region). The unit cell size is much smaller than the free space wavelength, and still smaller than one-third of the plasmonic wavelength. Therefore, it can be viewed as homogeneous to a good approximation within a unit cell. SPs are supported by an array of such unit cells with effective refractive index profile $N_{\text{eff}}(y,z)$. To clarify, n_{eff} is used to characterize uniform cells and N_{eff} is for patterned cells.

We next analyze how $N_{\text{eff}}(y,z)$ is modified by the patterns of unit cells with different molecules. For this purpose, we will use the EMT,³² commonly used to describe the effective refractive index of bulk waves in dielectric lattices. First, the homogeneous graphene patch with adsorption of one type of molecules is considered and the refractive indices are calculated as $n_{\text{eff}-1,2} = ck_{y-1,2}/\omega$ based on the dispersion relation of eq 4 for $n_{\text{eff}-1,2}$ values that correspond to the (TCNQ+TTF)-doped and (F4-TCNQ)-doped cases. The SPs act as the bulk wave propagating in a medium with refractive index equivalent to $n_{\text{eff}-1}$ or $n_{\text{eff}-2}$. Next, we consider subwavelength unit cells consisting of patches of two such regions. The effective refractive index of the unit cell is determined by the weighting average and can be written as

$$N_{\text{eff}} = (1 - \text{FF}^2)n_{\text{eff}-1} + \text{FF}^2n_{\text{eff}-2} \quad (5)$$

where $\text{FF} = a/b$ is the filling factor as shown in Figure 1. N_{eff} is shown in Figure 3 as a function of frequency for different FF values. Combinations of the two regions with different weights lead to different N_{eff} values varying within a large range. By

choosing proper FF value for each unit cell, any 2D index profile $N_{\text{eff}}(y,z)$ can be easily achieved.

We also carry out full-wave FDTD simulations to confirm the effective refractive index values obtained using periodically patterned unit cells, as a check of the results obtained from EMT. In the FDTD simulation, the atomic layer of graphene is replaced by an ultrathin layer of slab with thickness $\Delta = 6$ nm.¹⁵ The approximation of the thickness is examined in Figure S2 of Supporting Information and is small enough to exhibit the plasmonic properties supported by real graphene. Then the surface conductivities for (TCNQ+TTF)-doped case and (F4-TCNQ)-doped case are converted into the volume conductivities $\sigma = (\sigma_g)/\Delta$ as input parameters for different parts of the unit cell based on the FF. The period of the unit cell is set to 300 nm, smaller than one-third of the plasmonic wavelength at 10 THz. A broadband Gaussian pulse is used to excite all the possible modes with the central frequency of 10 THz. Given a set of wave vectors along y -direction, the frequencies of the eigenmodes are obtained by carrying out a discrete Fourier transform of the probed temporal spectrum at a given probe point. The effective refractive indices of the fundamental plasmonic modes are extracted from the dispersion relation between the given wave vector and the eigenfrequency [see Figure S4 of Supporting Information]. The effective refractive indices from FDTD simulation are plotted as dots in Figure 3 and are in excellent agreement with the results analytically calculated from EMT.

In contrast to plasmonic metamaterials that could be realized by the combination of a metallic layer on a GRIN dielectric substrate, functionalized graphene metamaterials exhibit special properties, particularly in the long wavelength limit, which we discuss next.

First, SPs bound to the surface of a metal (such as silver and gold) are 3D electron oscillations because electrons are free to move on the surface and into the bulk of the metallic layer. In contrast, graphene is a one-atom thick charge sheet that confines the electrons strictly to a 2D plane. The different types of electronic excitations in the two systems directly determine the characteristics of SPs. Specifically, the dispersion relation of SPs at the interface of gold and dielectric is given by $k_y = \omega/c[(\epsilon_m\epsilon_d)/(\epsilon_m + \epsilon_d)]^{1/2}$, where $\epsilon_m = \epsilon_\infty - [\omega_p^2/\omega(\omega + i\tau^{-1})]$ ($\epsilon_\infty = 1.53$, $\omega_p = 1.3 \times 10^{16}$ rad, $\tau = 5.6687 \times 10^{-14}$ s) is the dielectric constant of gold and ϵ_d is the dielectric constant for SiO₂ (air). The SP dispersion relation for a uniform gold–SiO₂ (air) interface is shown in the lower panel of Figure 2b. At the long wavelength limit, $|\epsilon_m| \gg |\epsilon_d|$, the dispersion relation

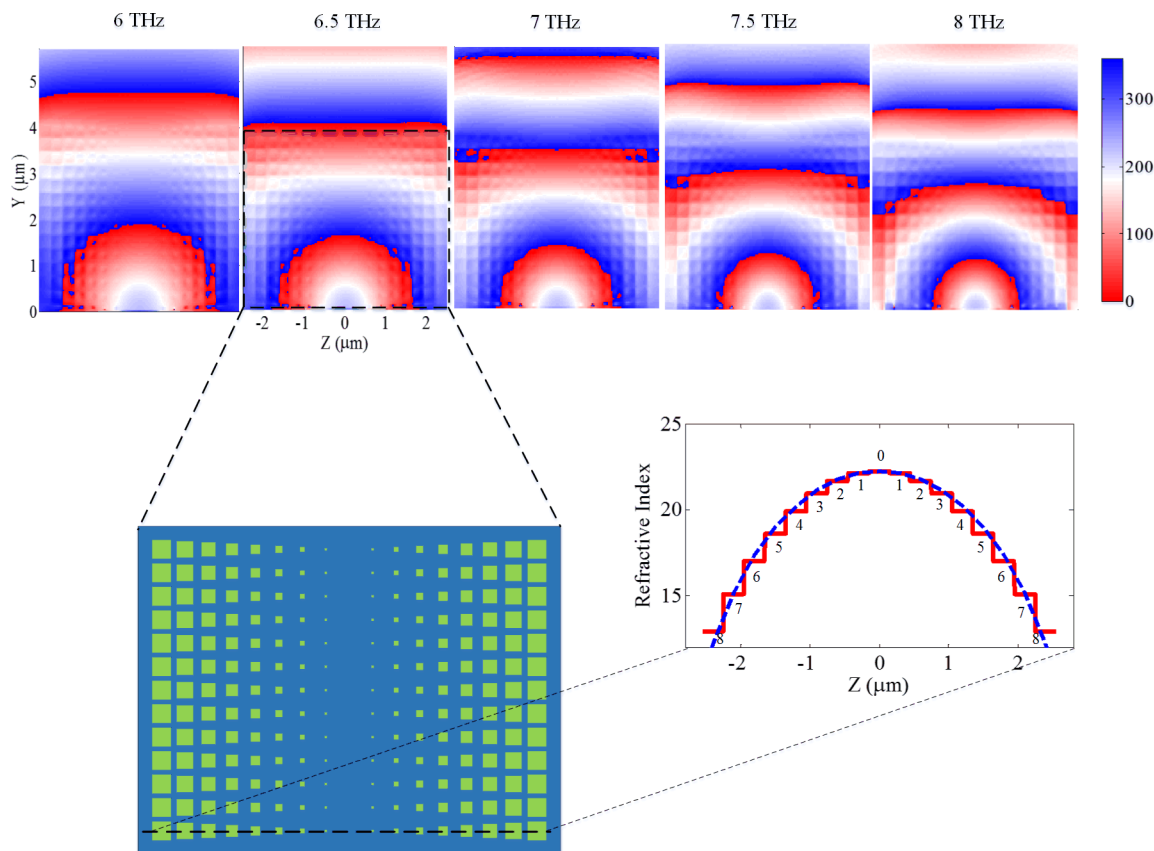


Figure 4. A Selfoc lens based on patterned graphene with organic molecules. The lower left panel shows the FDTD simulation grids with regions doped by adsorption of TCNQ + TTF molecules (blue) and F4-TCNQ molecules (green). The lower right panel shows the required smooth index profile and the designed stepped profile. The upper set of panels show the phase variation of the SPs passing through the flat Selfoc lens for frequencies in the 6–8 THz range. The point source is located at the center ($z = 0, y = 0$) of the bottom line. The waves propagate through the lens region (box surrounded by dashed black lines) and turn into plane waves.

simplifies to $k_y = (\omega/c)(\epsilon_d)^{1/2}$. The effective refractive index N_{eff} of the patterned unit cell is almost a constant in the long wavelength range, as shown in Figure 3b for different filling factors. In contrast to this behavior, the dispersion of 2D electron oscillations in graphene is characterized by a quadratic relation $\omega \propto (k_y)^{1/2}$ at the long wavelength limit,^{33,34} and N_{eff} is proportional to frequency $N_{\text{eff}} \propto \omega$. The tailored unit cells with different filling factors follow the linear trend shown in Figure 3a. Comparison of Figure 3a,b shows that N_{eff} is highly dispersive for a patterned-graphene-based unit cell, while it is nondispersive for a gold–dielectric-based metamaterial in the long wavelength limit. This difference originates from the features of 2D and 3D plasmonics mentioned above.

Second, due to the high conductivity of graphene the effective refractive index values in the patterned graphene can be 1 order of magnitude larger than the corresponding values of the gold–dielectric structure. The large effective refractive index requires ultrasmall unit cell size in order to behave as a locally homogeneous medium, which means that the unit cell size may be hundreds of nanometers although it operates in terahertz regime, enabling deep subwavelength structure. Meanwhile, the unit cell size is still well within the reach of current patterning methods like e-beam lithography.

Third, the values of N_{eff} for the gold–dielectric structure are bounded by the refractive index of the dielectric material, while they can go far beyond the refractive index of the dielectric part for the patterned graphene. Because graphene has all its atoms exposed on its surface, it is extremely sensitive to the

adsorption of molecules. The effective refractive index for FF = 0 is almost twice that of FF = 1. This provides a large tuning range since effective indices for other FF values will fall within this range.

Based in Figure 3a, any index profile $N_{\text{eff}}(y,z)$ can be readily achievable by choosing proper filling factors for two types of organic molecules patterned in each unit cell. Taking advantage of the versatile tunability of patterned graphene, we next design a Selfoc lens as a proof-of-concept for plasmonic GRIN applications with a quadratic index profile. Selfoc lenses are important elements for wave focusing and collimating and can also be used for spatial Fourier transform if the input signal and the probed signal are right at the focal planes before and after the lens.³⁵ To implement a plasmonic version of the Selfoc lens, the effective refractive index is uniform in y -direction and varies in z -direction as

$$N_{\text{eff}}(z) = N_{\text{eff}}(0) \sqrt{1 - \left(\frac{z}{R}\right)^2} \quad (6)$$

The index profile along the z -direction is specified by the smooth dash line in Figure 4 (lower right panel), and the surface wave is propagating in the y -direction. $N_{\text{eff}}(0)$ is the effective refractive index at the center in z -direction and R is the radius of curvature of the index profile. We use one full-wave FDTD simulation for the whole structure with a point source as the excitation at the frequency of 7 THz. The discretized index profile is indicated by the red solid line in Figure 4 (lower right

panel) with the FFs specified for each unit cell. There are 17 unit cells totally along z -direction, and 13 unit cells along y -direction with a period of 300 nm, as shown in Figure 4 (lower left panel). In the FDTD simulation, the 17×13 array is patterned exactly with two types of graphene, blue part and green part, with different conductivities resulting from adsorption of two types of molecules. FDTD grids with enough resolution in x -, y -, and z -directions are chosen to accurately simulate the whole structure. Because of the different phase velocities along the z -axis, the circular surface wave generated from the point source and bound to the surface gradually changes phase front and becomes a surface plane wave at the end of the lens, which is at a distance around $3.9 \mu\text{m}$ ($\sim \pi R/2$) from the point source.

The lens functions by design at the frequency 7 THz, but we also checked its broadband performance. In Figure 4 (top set of panels), the performance of the lens is plotted for frequencies from 6 to 8 THz. The collimating effects in this range are as good as at 7 THz with the same focal distance. It is interesting that despite the highly dispersive property of the effective refractive indices for the unit cell, the lens still works in a broadband range. For the functionalized graphene structure, the unit cell is a nonresonant one, but N_{eff} is linearly increasing with frequency. Because of this linearity, $(N_{\text{eff}}(zf_1))/(N_{\text{eff}}(zf_2)) = f_1/f_2 = (N_{\text{eff}}(0f_1))/(N_{\text{eff}}(0f_2))$. Thus $N_{\text{eff}}(z)$ and $N_{\text{eff}}(0)$ in eq 6 are scaled by the same factor f_1/f_2 and the radius of curvature R of the index profile remains the same when the frequency is changed, accommodating a broadband manipulation of the SPs with the same focal distance. From the aspect of EMT, the limit on bandwidth will be as follow. As the frequency increases from the designed 7 THz, the wavelength in free space is decreasing and N_{eff} is increasing, leading to the decrease of plasmonic wavelength with a higher speed. Hence there is an upper limit for the frequency where the EMT stops working if the plasmonic wavelength is reduced to a value comparable to the unit cell size. As the frequency decreases from 7 THz, we could expect that the plasmonic wavelength is increasing quickly, becoming even larger than the unit cell. The EMT works in a better condition. Obviously, one should be careful about the high loss due to Drude model contribution at very low frequency and high loss due to the molecular contribution at high frequencies.

In addition to the collimating application in Figure 4, the lens can surely be used for focusing and magnifying plasmonic waves when the propagation is in the opposite direction with plane wave excitation. Actually, it is an easy and common way to enhance the resolution and break the diffraction limit by choosing high refractive index materials for the lens. Functionalized graphene supports plasmonic waves with strongly shortened wavelength due to the large N_{eff} , which scales the diffraction limit to the order of $\lambda/2N_{\text{eff}}$. The entire designed lens is 2D atomically thin and its lateral size is only $0.1\lambda_0$ by $0.12\lambda_0$ where λ_0 is the free space wavelength at 7 THz, while most of the reported lenses^{36,37} have the dimensions comparable to wavelength or even larger. However, it is not easy to be used for imaging since the focusing and magnification effect is not in 3D space but confined on the surface. Nonetheless, such compact atomic-layer device size and the frequency regime make it an attractive approach for sensing applications in biology and pharmacology.

With the development of fabrication technology, the growth and transfer of large-area graphene sheet by chemical vapor deposition (CVD) are becoming mature and standardized

processes.^{38,39} The resolution of molecular patterning is well within the reach of e-beam lithography or dip-pen lithography either directly on graphene, or on the substrate, and putting the graphene layer on top of the patterned molecules later. These fabrication techniques enable the potential for experimental verification and practical implementation of functionalized graphene proposed in this paper. It is also worthy to note that it is not essential in practice to form a defect-free closely packed sample as we used in our model for carrying out the calculation. The performance of our devices is more sensitive to the averaged material property (surface conductivity) change in the diffraction limit, that is, a scale comparable to the plasmonic wavelength ($\sim 1 \mu\text{m}$) rather than the atomic-scale defects. Therefore, the demand for fabrication is realistic.

To summarize, we carried out a multiscale theoretical investigation to study functionalized graphene by organic molecules. The correlation between the electronic structure and the optical properties is analyzed and the device applications are explored. In general, this theoretical tool can be extended into other type of chemical dopants and even other 2D materials beyond graphene to explore new features of atomic layers and devices.

■ ASSOCIATED CONTENT

Supporting Information

Supporting Information contains the accuracy of the multiscale theory characterizing molecular-doped graphene system, the band structure of molecular doped graphene, the way to obtain effective refractive index of patterned graphene in FDTD, and the loss analysis for molecular doped graphene. This material is available free of charge via the Internet at <http://pubs.acs.org>.

■ AUTHOR INFORMATION

Corresponding Author

*E-mail: cheng.jie@husky.neu.edu.

Notes

The authors declare no competing financial interest.

■ ACKNOWLEDGMENTS

This work was supported in part by the U.S. Office of Naval Research (ONR) Grant N00014-10-1-0264. We acknowledge support from the Massachusetts Green High-Performance Computing Center (MGHPCC). We have used the Extreme Science and Engineering Discovery Environment (XSEDE) supported by NSF Grants TG-DMR120073 and TGPHY120034.

■ REFERENCES

- (1) Ma, H. F.; Chen, X.; Yang, X. M.; Jiang, W. X.; Cui, T. J. Design of multibeam scanning antennas with high gains and low side lobes using gradient-index metamaterials. *J. Appl. Phys.* **2010**, *107*, 014902.
- (2) Schurig, D.; Mock, J. J.; Justice, B. J.; Cummer, S. A.; Pendry, J. B.; Starr, A. F.; Smith, D. R. Metamaterial electromagnetic cloak at microwave frequencies. *Science* **2006**, *314*, 977–980.
- (3) Valentine, J.; Li, J. S.; Zentgraf, T.; Bartal, G.; Zhang, X. An optical cloak made of dielectrics. *Nat. Mater.* **2009**, *8*, 568–571.
- (4) Dhoubi, A.; Burokur, S. N.; de Lustrac, A.; Priou, A. Low-Profile Substrate-Integrated Lens Antenna Using Metamaterials. *IEEE Antennas Wireless Propag. Lett.* **2013**, *12*, 43–46.
- (5) Ni, X. J.; Emani, N. K.; Kildishev, A. V.; Boltasseva, A.; Shalae, V. M. Broadband Light Bending with Plasmonic Nanoantennas. *Science* **2012**, *335*, 427–427.
- (6) Smith, D. R.; Mock, J. J.; Starr, A. F.; Schurig, D. Gradient index metamaterials. *Phys. Rev. E* **2005**, *71*, 036609.

- (7) Liu, Y.; Zentgraf, T.; Bartal, G.; Zhang, X. Transformational Plasmon Optics. *Nano Lett.* **2010**, *10*, 1991–1997.
- (8) Renger, J.; Kadic, M.; Dupont, G.; Acimovic, S. S.; Guenneau, S.; Quidant, R.; Enoch, S. Hidden Progress: Broadband Plasmonic Invisibility. *Opt. Express* **2010**, *18*, 15757–15768.
- (9) Huidobro, P. A.; Nesterov, M. L.; Martin-Moreno, L.; Garcia-Vidal, F. J. Transformation Optics for Plasmonics. *Nano Lett.* **2010**, *10*, 1985–1990.
- (10) Ju, L.; Geng, B. S.; Horng, J.; Girit, C.; Martin, M.; Hao, Z.; Bechtel, H. A.; Liang, X. G.; Zettl, A.; Shen, Y. R.; Wang, F. Graphene plasmonics for tunable terahertz metamaterials. *Nat. Nanotechnol.* **2011**, *6*, 630–634.
- (11) Yan, H. G.; Li, X. S.; Chandra, B.; Tulevski, G.; Wu, Y. Q.; Freitag, M.; Zhu, W. J.; Avouris, P.; Xia, F. N. Tunable infrared plasmonic devices using graphene/insulator stacks. *Nat. Nanotechnol.* **2012**, *7*, 330–334.
- (12) Yan, H. G.; Low, T.; Zhu, W. J.; Wu, Y. Q.; Freitag, M.; Li, X. S.; Guinea, F.; Avouris, P.; Xia, F. N. Damping pathways of mid-infrared plasmons in graphene nanostructures. *Nat. Photonics* **2013**, *7*, 394–399.
- (13) Grigorenko, A. N.; Polini, M.; Novoselov, K. S. Graphene plasmonics. *Nat. Photonics* **2012**, *6*, 749–758.
- (14) Jablan, M.; Buljan, H.; Soljagic, M. Plasmonics in Graphene at Infrared Frequencies. *Phys. Rev. B* **2009**, *80*, 245435.
- (15) Vakil, A.; Engheta, N. Transformation Optics Using Graphene. *Science* **2011**, *332*, 1291–1294.
- (16) Hanson, G. W. Dyadic Green's Functions and Guided Surface Waves for a Surface Conductivity Model of Graphene. *J. Appl. Phys.* **2008**, *103*, 064302.
- (17) Huang, Y.; Wu, L. S.; Tang, M.; Mao, J. Design of a Beam Reconfigurable THz Antenna With Graphene-Based Switchable High-Impedance Surface. *IEEE Trans. Nanotechnol.* **2012**, *11*, 836–842.
- (18) Fallahi, A.; Perruisseau-Carrier, J. Design of tunable bi-periodic graphene metasurfaces. *Phys. Rev. B* **2012**, *86*, 195408.
- (19) Lu, Z. L.; Zhao, W. S. Nanoscale electro-optic modulators based on graphene-slot waveguides. *J. Opt. Soc. Am. B* **2012**, *29*, 1490–1496.
- (20) Lee, S. H.; Choi, M.; Kim, T.-T.; Lee, S.; Liu, M.; Yin, X.; Choi, H. K.; Lee, S. S.; Choi, C.-G.; Choi, S.-Y.; Zhang, X.; Min, B. Switching Terahertz Waves with Gate-Controlled Active Graphene Metamaterials. *Nat. Mater.* **2012**, *11*, 936–941.
- (21) Fedorov, A. The all-organic route to doping graphene. *Physics* **2010**, *3*, 46.
- (22) Pinto, H.; Jones, R.; Goss, J. P.; Briddon, P. R. p-type doping of graphene with F4-TCNQ. *J. Phys.: Condens. Matter* **2009**, *21*, 402001.
- (23) Sun, J. T.; Lu, Y. H.; Chen, W.; Feng, Y. P.; Wee, A. T. S. Linear tuning of charge carriers in graphene by organic molecules and charge-transfer complexes. *Phys. Rev. B* **2010**, *81*, 155403.
- (24) Georgakilas, V.; Otyepka, M.; Bourlinos, A. B.; Chandra, V.; Kim, N.; Kemp, K. C.; Hobza, P.; Zboril, R.; Kim, K. S. Functionalization of Graphene: Covalent and Non-Covalent Approaches, Derivatives and Applications. *Chem. Rev.* **2012**, *112*, 6156–6214.
- (25) Kresse, G.; Joubert, D. From ultrasoft pseudopotentials to the projector augmented-wave method. *Phys. Rev. B* **1999**, *59*, 1758–1775.
- (26) Soler, J. M.; et al. The SIESTA method for ab initio order-N materials simulation. *J. Phys.: Condens. Matter* **2002**, *14*, 2745–2779.
- (27) Kaxiras, E. *Atomic and Electronic Structure of Solids*; Cambridge University Press: Cambridge, 2003.
- (28) Novoselov, K. S.; Geim, A. K.; Morozov, S. V.; Jiang, D.; Zhang, Y.; Dubonos, S. V.; Grigorieva, I. V.; Firsov, A. A. Electric Field Effect in Atomically Thin Carbon Films. *Science* **2004**, *306*, 666–669.
- (29) Maksimov, E. G.; Mazin, I. I.; Rashkeev, S. N.; Yu, A. U. First-principles calculations of the optical properties of metals. *J. Phys. F: Met. Phys.* **1988**, *18*, 833–849.
- (30) Falkovsky, L. A.; Pershoguba, S. S. Optical far-infrared properties of a graphene monolayer and multilayer. *Phys. Rev. B* **2007**, *76*, 153410.
- (31) Gan, C. H.; Chu, H. S.; Li, E. P. Synthesis of highly confined surface plasmon modes with doped graphene sheets in the midinfrared and terahertz frequencies. *Phys. Rev. B* **2012**, *85*, 125431.
- (32) Brauer, R.; Bryngdahl, O. Design of Antireflection Gratings with Approximate and Rigorous Methods. *Appl. Opt.* **1994**, *33*, 7875–7882.
- (33) Nagao, T.; Hildebrandt, T.; Henzler, M.; Hasegawa, S. Dispersion and Damping of a Two-Dimensional Plasmon in a Metallic Surface-State Band. *Phys. Rev. Lett.* **2001**, *86*, 5747–5750.
- (34) Hwang, E. H.; DasSarma, S. Dielectric function, screening, and plasmons in two-dimensional graphene. *Phys. Rev. B* **2007**, *75*, 205418.
- (35) Vakil, A.; Engheta, N. Fourier optics on graphene. *Phys. Rev. B* **2012**, *85*, 075434.
- (36) Lee, J. Y.; Hong, B. H.; Kim, W. Y.; Min, S. K.; Kim, Y.; Jouravlev, M. V.; Bose, R.; Kim, K. S.; Hwang, I.-C.; Kaufman, L. J.; Wong, C. W.; Kim, P.; Kim, K. S. Near-field focusing and magnification through self-assembled nanoscale spherical lenses. *Nature* **2009**, *460*, 498–501.
- (37) Mason, D. R.; Jouravlev, M. V.; Kim, K. S. Enhanced resolution beyond the Abbe diffraction limit with wavelength-scale solid immersion lenses. *Opt. Lett.* **2010**, *35*, 2007–2009.
- (38) Li, X. S.; Cai, W. W.; An, J. H.; Kim, S.; Nah, J.; Yang, D. X.; Piner, R.; Velamakanni, A.; Jung, I.; Tutuc, E.; Banerjee, S. K.; Colombo, L.; Ruoff, R. S. Large-Area Synthesis of High-Quality and Uniform Graphene Films on Copper Foils. *Science* **2009**, *324*, 1312–1314.
- (39) Kim, K. S.; Zhao, Y.; Jang, H.; Lee, S. Y.; Kim, J. M.; Kim, K. S.; Ahn, J. H.; Kim, P.; Choi, J. Y.; Hong, B. H. Large-scale pattern growth of graphene films for stretchable transparent electrodes. *Nature* **2009**, *457*, 706–710.